ISSN 1070-3284, Russian Journal of Coordination Chemistry, 2021, Vol. 47, No. 11, pp. 769–779. © The Author(s), 2021. This article is an open access publication.
Russian Text © The Author(s), 2021, published in Koordinatsionnaya Khimiya, 2021, Vol. 47, No. 11, pp. 707–716.

Binding of Gold(III) from Solutions by the $[Ag_6\{S_2CN(CH_2)_6\}_6]$ Cluster: Synthesis, Thermal Behavior, and Self-Organization of the Supramolecular Structure of the Double Complex $[Au\{S_2CN(CH_2)_6\}_2]_2[AgCl_2]Cl{\cdot}2CHCl_3$ (Role of Secondary Au···Cl, Ag···S, and Cl···Cl Interactions)

E. V. Korneeva[a], E. V. Novikova[a], O. V. Loseva[a], A. I. Smolentsev[b, c], and A. V. Ivanov[a, *]

[a] *Institute of Geology and Nature Management, Far Eastern Branch, Russian Academy of Sciences, Blagoveshchensk, 675000 Russia*

[b] *Nikolaev Institute of Inorganic Chemistry, Siberian Branch, Russian Academy of Sciences, Novosibirsk, 630090 Russia*

[c] *Novosibirsk State University, Novosibirsk, 630090 Russia*

**e-mail: alexander.v.ivanov@chemist.com*

Received February 4, 2021; revised March 15, 2021; accepted March 22, 2021

Abstract—The capability of silver(I) *cyclo*-hexamethylenedithiocarbamate to concentrate gold(III) from solutions characterized by a high level of salinity (5.15 M NaCl) into the solid phase has been established. The double chloroform-solvated Au(III)–Ag(I) complex $[Au\{S_2CN(CH_2)_6\}_2]_2[AgCl_2]Cl{\cdot}2CHCl_3$ (**I**) was preparatively isolated as an individual form of binding of $[AuCl_4]^-$ anions. The composition of the ionic structural units of compound **I** indicates that gold(III) binding from a solution to the solid phase is accompanied by the complete redistribution of the HmDtc ligands between the coordination spheres of Ag(I) and Au(III). Complex **I** characterized by IR spectroscopy, simultaneous thermal analysis, and X-ray structure analysis (CIF file CCDC no. 2051654) exhibits the supramolecular structure containing two oppositely charged pseudo-polymeric subsystems. Complex cations $[Au\{S_2CN(CH_2)_6\}_2]^+$ and anions $[AgCl_2]^-$ (in a ratio of 2 : 1) form a complicatedly organized cation-anionic pseudo-polymeric ribbon $(\{[Au(HmDtc)_2]\cdots[AgCl_2]\cdots[Au(HmDtc)_2]\}^+)_n$ due to secondary interactions Ag···S (3.2613 Å) and Au···Cl (3.2765 Å). The pseudo-polymeric ribbon consists of two rows of cations and a row of anions. The outer-sphere chloride ions combine the solvate chloroform molecules by two equivalent hydrogen bonds Cl···H–C yielding anion-molecular triads $[Cl_3CH\cdots Cl\cdots HCCl_3]^-$, which are involved in the formation of the supramolecular ribbon due to the secondary Cl···Cl interactions (3.4058 Å) between the nonequivalent chlorine atoms of the nearest solvate molecules. The study of the thermal behavior of complex **I** makes it possible to determine the character of thermolysis and conditions for the quantitative regeneration of bound gold.

Keywords: gold(III)–silver(I) double complexes, pseudo-polymeric compounds, supramolecular self-organization, secondary interactions (Ag···S, Au···Cl, Cl···Cl), thermal behavior

DOI: 10.1134/S1070328421090050

INTRODUCTION

Silver(I) dithiocarbamate (Dtc) complexes are convenient precursors for the preparation of both acanthite (α-Ag_2S) films and nanopowders [1–4] and Janus nanoparticles Ag_2S/Ag^0 (including a combination of the metal and metal sulfide) [5, 6], which are of practical interest for microelectronics. Since Ag_2S is characterized by low toxicity and high stability in biological media, it is promising to use it in medicine for manufacturing biocompatible nanoprobes [7, 8]. It is noteworthy that a low toxicity of silver against cells of mammals compared to other metals is combined in a unique manner with a high toxicity against microorganisms [9]. In addition, we have previously found the capability of silver(I) dialkyldithiocarbamates to bind gold(III) from solutions into the solid phase, forming pseudo-polymeric heterometallic Au(III)–Ag(I) compounds of the ionic type with the complicatedly organized supramolecular structures [10, 11]. Compounds of this type can be of interest as precursors of gold nanoparticles and thin films, which are promising for practical use in diverse areas [12–15], and of Janus particles of the Ag_2S/Au^0 type [16].

Continuing the above research, in this work we studied the reaction of the hexanuclear silver(I) *cyclo*-hexamethylenedithiocarbamate (HmDtc) cluster, whose structure was determined earlier [17], with

$AuCl_3$ in a 5.15 M solution of NaCl. Bis(*N*,*N*-*cyclo*-hexamethylenedithiocarbamato-*S*,*S*')gold(III) dichloroargentate chloride solvated by chloroform of the composition $[Au\{S_2CN(CH_2)_6\}_2]_2[AgCl_2]Cl\cdot 2CHCl_3$ (**I**) was preparatively isolated from the reaction products as the form of binding gold(III). The structural organization, thermal behavior, and spectral characteristics of compound **I** were studied by single-crystal X-ray diffraction (XRD) analysis, simultaneous thermal analysis (STA), and IR spectroscopy.

EXPERIMENTAL

Sodium *N*,*N*-*cyclo*-hexamethylenedithiocarbamate $Na\{S_2CN(CH_2)_6\}\cdot 2H_2O$ was synthesized by the reaction of hexamethyleneimine (Aldrich) with carbon sulfide (Merck) in an alkaline medium [18]. The initial silver(I) complex $[Ag_6\{S_2CN(CH_2)_6\}_6]$ was synthesized using a described procedure [17].

Synthesis of complex I was carried out using the reaction of freshly precipitated $[Ag_6\{S_2CN(CH_2)_6\}_6]$ with $AuCl_3$ in a 5.15 M solution of NaCl (which is close to the saturation conditions at 20°C). Taking into account the determined composition and structure of complex **I**, we can present the heterogeneous reaction of gold(III) binding from a solution to the solid phase with the formation of intermediate substance **Ia** as follows:

$$2\left[Ag_6\left\{S_2CN(CH_2)_6\right\}_6\right] + 6Na[AuCl_4] + 3NaCl = 3[Au\{S_2CN(CH_2)_6\}_2]_2[AgCl_2]Cl\ (\mathbf{Ia}) + 9Na[AgCl_2].$$

A solution (10 mL) of $Na[AuCl_4]$ containing gold(III) (34.9 mg, 0.177 mmol) was poured to freshly precipitated $[Ag_6\{S_2CN(CH_2)_6\}_6]$ (100 mg, 0.059 mmol), and the mixture was stirred at 60°C for 1 h. The greenish-yellow color of the precipitate changed rapidly to red-orange during the first minutes of its interaction with the solution, and further the precipitate turned saturated yellow-orange with the simultaneous decoloring of the solution of gold(III). The degree of binding of gold from solutions to the solid phase was 99.89%, indicating the formation of new compounds in the solid phase. (The residual content of gold in the solution after extraction was determined on an atomic absorption spectrometer Hitachi, model 180–50, class 1). The obtained precipitate of compound **Ia** was filtered off, washed with water, and dried on a filter. The single crystals of compound **I** suitable for XRD were obtained by the dissolution of the precipitate in an acetone–chloroform (1 : 1) mixture followed by the slow evaporation of the solvents at room temperature. The yield of the yellow-orange prismatic crystals of compound **I** was 79.4%.

For $C_{30}H_{50}N_4S_8Cl_9AgAu_2$			
Anal. calcd., %	C, 23.33	H, 3.26	N, 3.62
Found, %	C, 23.47	H, 3.41	N, 3.53

IR for **I** (KBr), ν, cm^{-1}: 2926 s, 2885 s, 2844 m, 1542 vs, 1459 m, 1438 s, 1365 w, 1358 w, 1346 w, 1290 w, 1276 m, 1206 m, 1162 s, 1094 w, 1058 w, 1007 w, 993 w, 978 w, 959 w, 902 w, 879 w, 847 w, 829 vw, 825 vw, 810 w, 750 s, 743 s, 657 m, 625 m, 563 w, 459 w.

IR for **Ia** (KBr), ν, cm^{-1}: 2920 s, 2849 m, 1542 s, 1492 m, 1473 w, 1441 w, 1421 s, 1362 m, 1344 w, 1270 s, 1242 w, 1194 m, 1160 s, 1092 m, 1056 w, 1045 w, 1004 w, 994 w, 973 m, 938 m, 904 w, 877 w, 846 w, 823 w, 745 w, 623 w, 568 w, 461 w.

The IR spectra of the synthesized substances pressed in KBr pellets were recorded at room temperature on an FSM-1201 interferential FT-IR spectrometer in a range of 400–4000 cm^{-1} (FSpec software, version 4.0.0.2 for Windows, OOO Monitoring, Russia).

XRD was carried out for a prismatic single crystal of compound **I** on a Bruker-Nonius X8 Apex CCD diffractometer (MoK_α radiation, $\lambda = 0.71073$ Å, graphite monochromator) at 150(2) K. The data were collected using a standard procedure: φ and ω scan modes of narrow frames. An absorption correction was applied empirically using the SADABS program [19]. The structure was determined by a direct method and refined by least squares (for F^2) in the full-matrix anisotropic approximation of non-hydrogen atoms using the SHELXL-2018/3 program [20]. The positions of the hydrogen atoms in the HmDtc ligands and solvate $CHCl_3$ molecules were geometrically calculated and included into refinement by the riding model. The main crystallographic data and structure refinement results for compound **I** are presented in Table 1. Selected bond lengths and angles are given in Table 2. The geometric parameters of the C–H···Cl hydrogen bonds and Cl···Cl secondary interactions are listed in Table 3.

The atomic coordinates, bond lengths, and angles were deposited with the Cambridge Crystallographic Data Centre (CIF file CCDC no. 2051654 (**I**); deposit@ccdc.cam.ac.uk or http://www.ccdc.cam.ac.uk).

The thermal behavior of compound **I** was studied by the STA method including the parallel detection of thermogravimetry (TG) and differential scanning calorimetry (DSC) curves. The study was carried out on

Table 1. Crystallographic data and experimental and structure refinement parameters for complex **I**

Parameter	Value
Empirical formula	$C_{30}H_{50}N_4S_8Cl_9AgAu_2$
FW	1544.07
Crystal system	Monoclinic
Space group	*P*2/*c*
a, Å	20.0396(6)
b, Å	6.06430(10)
c, Å	20.4313(6)
β, deg	92.8030(10)
V, Å^3	2479.97(11)
Z	2
ρ_{calc}, g/cm^3	2.068
μ, mm^{-1}	7.143
F(000)	1488
Crystal size, mm^3	0.12 × 0.10 × 0.02
Range of data collection over θ, deg	2.00–27.60
Ranges of reflection indices	$-26 \le h \le 25$, $-7 \le k \le 6$, $-25 \le l \le 26$
Measured reflections	15977
Independent reflections (R_{int})	5702 (0.0388)
Reflections with $I > 2\sigma(I)$	4629
Refinement variables	245
GOOF	0.954
R factors for $F^2 > 2\sigma(F^2)$	$R_1 = 0.0277$, $wR_2 = 0.0514$
R factors for all reflections	$R_1 = 0.0423$, $wR_2 = 0.0545$
Residual electron density (min/max), e/Å^3	−0.709/1.263

an STA 449C Jupiter instrument (NETZSCH) in corundum crucibles under caps with holes providing a vapor pressure of 1 atm during the thermal decomposition of the sample. The heating rate was 5°C/min to 1100°C under an argon atmosphere. The weight of the samples was 2.528–7.840 mg. The accuracy of temperature measurements was ±0.6°C, and that of the weight change was $\pm 1 \times 10^{-4}$ mg. A correction file and temperature and sensitivity calibrations for the specified temperature program and heating rate were used when recording the TG and DSC curves. The independent determination of the melting point was carried out on a PTP(M) instrument (OAO Khimlaborpribor, Russia).

RESULTS AND DISCUSSION

The strong interaction of vibrations of the C–H, C–C, and C–N bonds in the HmDtc ligands predetermines a complicated IR spectral pattern of complex **I** and substance **Ia**. Therefore, when analyzing the spectrum, we additionally used the IR spectral data for the initial $[Ag_6\{S_2CN(CH_2)_6\}_6]$ cluster [17], sodium *cyclo*-hexamethylenedithiocarbamate dihydrate $Na\{S_2CN(CH_2)_6\}\cdot 2H_2O$ [21], hexamethyleneimine $C_6H_{12}NH$ [22], cycloheptane C_7H_{14} [23], and chloroform $CHCl_3$.[1] The IR spectra of compounds **I**/**Ia** exhibit absorption bands at 2926/2920 and 2844/2849 cm^{-1} due to stretching vibrations $\nu_{as}(CH_2)$ and $\nu_s(CH_2)$, respectively. The medium-intensity absorption band at 1459/1473 cm^{-1} corresponds to the bending (scissor) vibrations δ_s of the $-CH_2-$ groups. The high-intensity band at 1162/1160 cm^{-1} corresponds to the stretching vibrations of the $N-CH_2$ bonds. The close positions of the corresponding absorption bands in the IR spectra of sodium hexamethylenedithiocar-

[1] The liquid membrane method [24], in which a droplet of the studied liquid is compressed between two KBr plates, was used for recording the IR spectrum in $CHCl_3$ (3018 m, 1219 s, 772 vs, 668 m; cm^{-1}).

Table 2. Selected bond lengths (*d*) and bond (ω) and torsion (φ) angles in the structure of complex **I***

Cation			
Bond	*d*, Å	Bond	*d*, Å
Au(1)–S(1)	2.3465(10)	N(2)–C(9)	1.474(4)
Au(1)–S(2)	2.3333(10)	N(2)–C(14)	1.482(4)
Au(1)–S(3)	2.3333(10)	C(2)–C(3)	1.530(5)
Au(1)–S(4)	2.3442(10)	C(3)–C(4)	1.522(6)
Au(1)···Cl(1)	3.2765(9)	C(4)–C(5)	1.530(5)
S(1)–C(1)	1.738(4)	C(5)–C(6)	1.536(5)
S(2)–C(1)	1.739(4)	C(6)–C(7)	1.507(5)
S(3)–C(8)	1.737(4)	C(9)–C(10)	1.523(5)
S(4)–C(8)	1.727(4)	C(10)–C(11)	1.518(5)
N(1)–C(1)	1.294(5)	C(11)–C(12)	1.521(5)
N(1)–C(2)	1.472(4)	C(12)–C(13)	1.536(5)
N(1)–C(7)	1.490(5)	C(13)–C(14)	1.512(6)
N(2)–C(8)	1.306(5)		
Angle	ω, deg	Angle	ω, deg
S(1)Au(1)S(2)	75.25(3)	Au(1)S(1)C(1)	86.76(13)
S(1)Au(1)S(3)	104.58(3)	Au(1)S(2)C(1)	87.04(13)
S(1)Au(1)S(4)	177.53(3)	Au(1)S(3)C(8)	86.83(13)
S(2)Au(1)S(3)	179.61(3)	Au(1)S(4)C(8)	86.70(13)
S(2)Au(1)S(4)	104.85(3)	S(1)C(1)S(2)	110.6(2)
S(3)Au(1)S(4)	75.31(3)	S(3)C(8)S(4)	111.1(2)
Angle	φ, deg	Angle	φ, deg
Au(1)S(1)S(2)C(1)	−173.5(2)	Au(1)S(3)S(4)C(8)	−177.8(2)
S(1)Au(1)C(1)S(2)	−174.1(2)	S(3)Au(1)C(8)S(4)	−178.1(2)
S(1)C(1)N(1)C(2)	0.2(5)	S(3)C(8)N(2)C(9)	0.6(4)
S(1)C(1)N(1)C(7)	176.0(3)	S(3)C(8)N(2)C(14)	179.7(2)
S(2)C(1)N(1)C(2)	−178.2(3)	S(4)C(8)N(2)C(9)	−178.3(2)
S(2)C(1)N(1)C(7)	−2.3(5)	S(4)C(8)N(2)C(14)	0.7(5)
C(4)C(3)C(2)N(1)	−77.2(4)	C(11)C(10)C(9)N(2)	73.0(4)
C(5)C(6)C(7)N(1)	−50.6(5)	C(12)C(13)C(14)N(2)	42.9(4)
C(4)C(5)C(6)C(7)	87.8(4)	C(11)C(12)C(13)C(14)	−86.9(4)
C(3)C(4)C(5)C(6)	−68.1(4)	C(10)C(11)C(12)C(13)	67.2(4)
Anion			
Bond	*d*, Å	Bond	*d*, Å
Ag(1)–Cl(1)	2.3497(11)	Ag(1)···S(2)[b]	3.2613(10)
Angle	ω, deg	Angle	ω, deg
Cl(1)–Ag(1)–Cl(1)[a]	179.38(5)	Cl(1)–Ag(1)···S(2)[c]	101.53(3)
Cl(1)–Ag(1)···S(2)[b]	78.98(3)	S(2)[b]···Ag(1)···S(2)[c]	73.07(2)

* Symmetry transforms: [a] $-x, y, 1/2 - z$; [b] $x, y - 1, z$; [c] $-x, y - 1, 1/2 - z$.

Table 3. Geometric parameters of the C–H···Cl hydrogen bond and Cl···Cl interaction in complex **I**

Contact D–X···A	Distance, Å			Angle D–X···A, deg
	D–X	X···A	D···A	
C(15)–H(15)···Cl(5)	1.00	2.34	3.341(4)	176
C(15)–Cl(4)···Cl(3)[a]	1.765(4)	3.4058(15)	5.158(4)	171.7(1)
C(15)[a]–Cl(3)[a]···Cl(4)			4.433(4)	114.2(1)

* Symmetry transforms: [a] $x, y - 1, z$.

bamate dihydrate, complex **I**, and substance **Ia** indicate that the main structural features of the peripheral cyclic $-N(CH_2)_6$ fragment is retained upon complexation. The most noticeable distinctions are characteristic of the stretching vibrations of the –C(S)S– groups directly bound with the central metal atom and of the partially double bond N–C(S)S. The relative intensity of the bands at 1058/1056 and 978/973 cm^{-1} caused by the $\nu_{as}(CS_2)$ and $\nu_s(CS_2)$ vibrations, respectively, decreases substantially upon the binding of the HmDtc ligands by the central metal atom, which can be related to an increase in the contribution of the covalent component to the discussed bonds (decrease in their polarity) due to the shift of the electron density from the metal to sulfur atoms. At the same time, the most intense absorption bands in the IR spectra of compounds **I** and **Ia** caused by the stretching vibrations of the N–C bonds in the dithiocarbamate groups are significantly shifted to the high-frequency range (1542 and 1542 cm^{-1}) compared to the initial cluster $[Ag_6\{S_2CN(CH_2)_6\}_6]$ (1494 cm^{-1} [17]) and $Na\{S_2CN(CH_2)_6\}\cdot 2H_2O$ (1485 cm^{-1} [21]). Thus, all absorption bands discussed lie between the frequency ranges of the ordinary ν(C–N) (1350–1250 cm^{-1}) and double ν(C=N) (1690–1640 cm^{-1}) bonds, indicating a substantial contribution of double bonding to the formally ordinary N–C(S)S bonds [25]. However, according to the data obtained, much shorter N–C(S)S bonds than those in the initial silver(I) complex (1.335 Å [17]) are expected for complex **I**.

The presence of the solvate chloroform molecules in the structure of complex **I** is indicated by absorptions observed in two ranges of the IR spectrum (~3000 and ~800–600 cm^{-1}): (a) the band at 2885 cm^{-1} corresponding to the ν(C–H) stretching vibrations (it should be mentioned that the usually relatively weak absorption band of the methine group in the spectrum of compound **I** exhibits a high intensity, which is caused by a significant polarity of the C–H bond and the presence of a dipole moment in the $CHCl_3$ molecule) and (b) two (1 : 1) closely lying high-intensity $\nu_{as}(C-Cl)$ bands at 750 and 743 cm^{-1} and the medium-intensity $\nu_s(C-Cl)$ band at 657 cm^{-1}.

The direct XRD method was used to determine the structural organization of the solvated heteronuclear Au(III)–Ag(I) complex (compound **I**). The unit cell of the studied compound includes two formula units $[Au\{S_2CN(CH_2)_6\}_2][AgCl_2]Cl\cdot 2CHCl_3$ (Fig. 1). Thus, the noncentrosymmetric $[Au\{S_2CN(CH_2)_6\}_2]^+$ cations (Fig. 2a), $[AgCl_2]^-$ anions (Fig. 2b), whose geometry is nearly linear (*sp*-hybrid state of the silver atom), outer-sphere Cl^- anions, and solvate $CHCl_3$ molecules, each containing three nonequivalent chlorine atoms (Cl(2), Cl(3), and Cl(4)), are the structural units of the complex.

In the complex gold(III) cation, the coordination of two nonequivalent HmDtc ligands, close to the *S*,*S*'-isobidentate mode (the Au–S bond lengths range from 2.3333 to 2.3465 Å), results in the formation of the bicyclic system $[CS_2AuS_2C]$ containing two four-membered metallocycles with the common metal atom. However, the Au–S–S–C and S–Au–C–S torsion angles (Table 2) indicate that the atoms are nearly coplanar in one of the discussed $[AuS_2C]$ metallocycles, whereas the second cycle is characterized by some tetrahedral distortion due to which the diagonal S(1)–Au–S(4) angle somewhat deviates from 180°. The geometry of the $[AuS_4]$ chromophore is close to the planar-tetragonal one, indicating the inner-orbital dsp^2-hybrid state of the gold atom. As expected from the IR spectral data, the N–C(S)S bonds in complex **I** (1.294 and 1.306 Å) are significantly shorter than those in the initial silver(I) cluster [17]. The S_2C-NC_2 structural fragments in the HmDtc ligands are nearly planar, which is indicated by the values of the corresponding torsion angles close to 0° or 180° (Table 2). A specific feature of the $[Au\{S_2CN(CH_2)_6\}_2]^+$ cation (Fig. 2a) is the spatial localization of the seven-membered cyclic fragments $-N(CH_2)_6$ at one side from the medium plane of the central bicyclic fragment (*cis* orientation). In spite

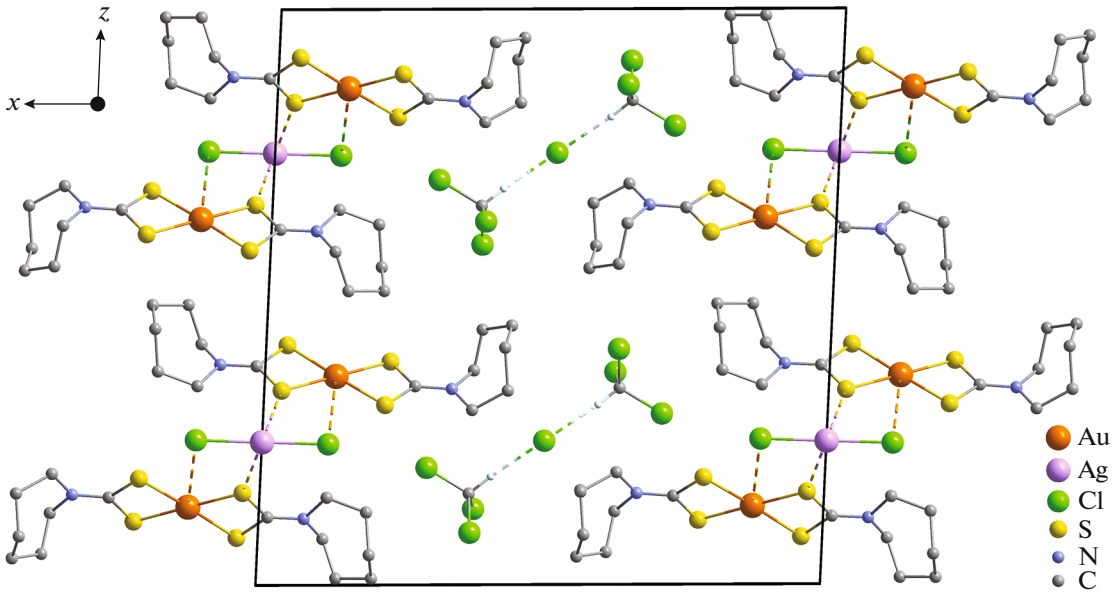

Fig. 1. Projection of the structure of compound **I** on the *xz* plane. The hydrogen atoms in the HmDtc ligands are omitted. The secondary Au···Cl and Ag···S interactions and C–H···Cl hydrogen bonds are shown by dashed lines.

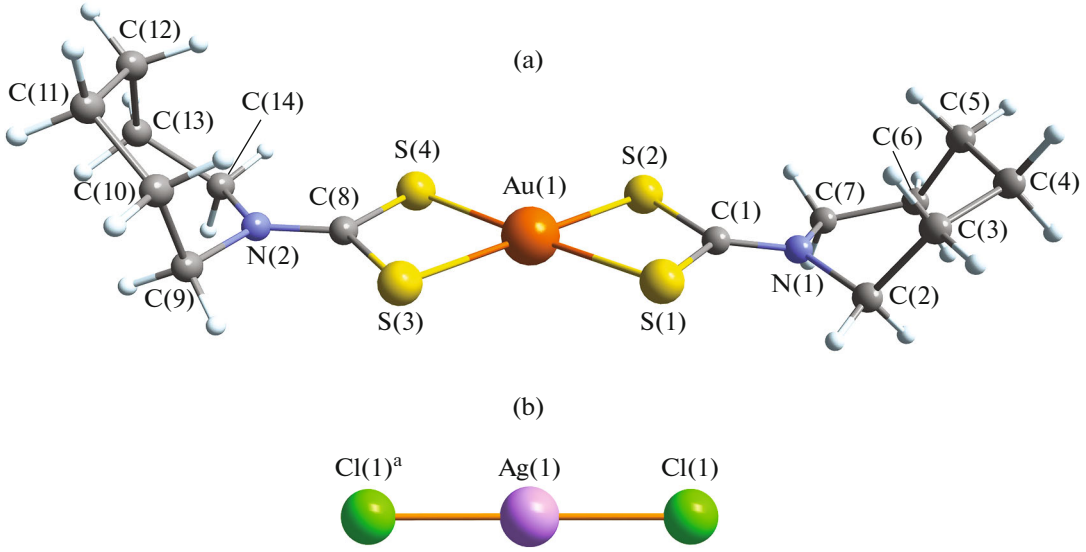

Fig. 2. Structures of the (a) $[Au\{S_2CN(CH_2)_6\}_2]^+$ complex cation and (b) $[AgCl_2]^-$ linear anion. Symmetry transforms: [a] $-x, y, 1/2 - z$.

of differences in the geometric characteristics of the $-N(CH_2)_6$ seven-membered heterocyclic fragments of the nonequivalent HmDtc ligands (see the corresponding torsion angles in Table 2), both can be approximated by the "twist-chair" conformations [26–28].

Compound **I** is characterized by a complicated supramolecular structure including two pseudopolymeric subsystems, which are formed due to the secondary interactions (Au···S, Au···Cl, Cl···Cl) [29] and hydrogen bonds C–H···Cl. In the cation-anionic subsystem $(\{[Au(HmDtc)_2]_2[AgCl_2]\}^+)_n$ (Fig. 3), each dichloroargentate(I) ion interacts with four nearest gold(III) cations to form two pairs of equivalent secondary bonds Ag(1)···S(2)[b/c] (3.2613 Å) and Au(1)···Cl(1), Au(1)[a]···Cl(1)[a] (3.2765 Å). The sum of the van der Waals radii of the corresponding pairs of atoms (3.52 and 3.41 Å [30]) appreciably exceeds the length of the presented secondary bonds. In turn, each $[Au\{S_2CN(CH_2)_6\}_2]^+$ cation is linked by the second-

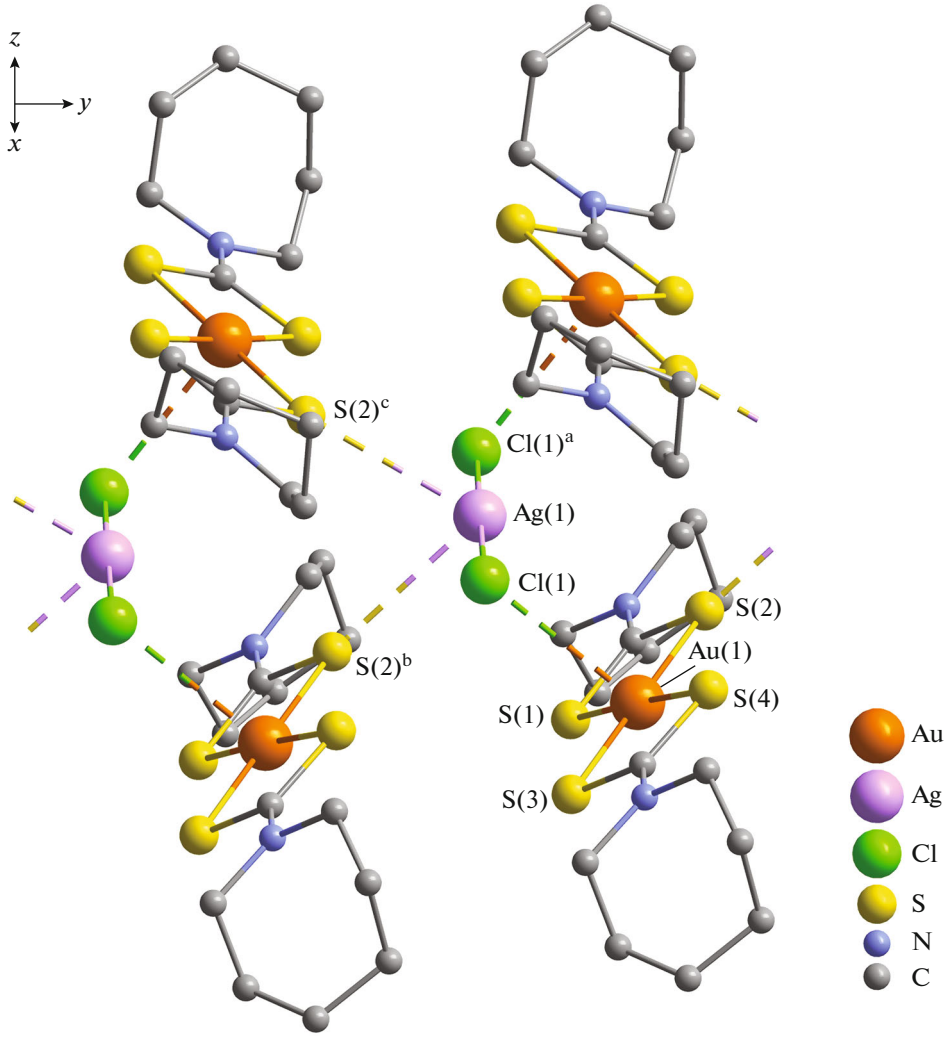

Fig. 3. Fragment of the cation-anionic pseudo-polymeric ribbon $(\{[Au(HmDtc)_2]_2[AgCl_2]\}^+)_n$ oriented along the *y* axis. The Au···Cl and Ag···S secondary bonds are shown by dashed lines. Symmetry transforms: [a] $-x, y, 1/2 - z$; [b] $x, y - 1, z$; [c] $-x, y - 1, 1/2 - z$.

ary interactions with two $[AgCl_2]^-$ anions, thus forming a supramolecular ribbon directed along the *y* axis, which includes two rows of complex gold(III) cations and a row of silver(I) anions.

The outer-sphere Cl^- ion and solvate chloroform molecules participate in the formation of the second pseudo-polymeric subsystem. Both $CHCl_3$ molecules solvate the chloride ion to form equivalent hydrogen bonds C(15)–H(15)···Cl(5) and C(15)[b]–H(15)[b]··· Cl(5), resulting in the building of the anion-molecular triad $[Cl_3C–H···Cl···H–CCl_3]^-$ (Fig. 4, Table 3). In turn, the intermolecular pair secondary interactions[2] Cl···Cl occur between the adjacent triads, the Cl(3) and Cl(4) atoms of each $CHCl_3$ molecule are involved in the Cl···Cl interactions (Fig. 5, Table 3), and the Cl(4)···Cl(3)[a], Cl(4)[b]···Cl(3)[c] distance is 3.4058 Å, which is shorter by 0.1 Å than the doubled van der Waals radius of the chlorine atom (3.50 Å [30]). A set of the discussed interactions results in the formation of the second, anion-molecular pseudo-polymeric ribbon of the $([Cl_3C–H···Cl···H–CCl_3]^-)_n$ composition. Thus, the supramolecular structure of compound **I** includes two oppositely charged pseudo-polymeric subsystems.

Two main types of secondary interhalogen interactions differed in the geometry of the corresponding structural fragment are considered [31–33]. The first type is characterized by an approximate equality of the

[2] The discussed interactions are based on different characters of polarization of the involved chlorine atoms [31].

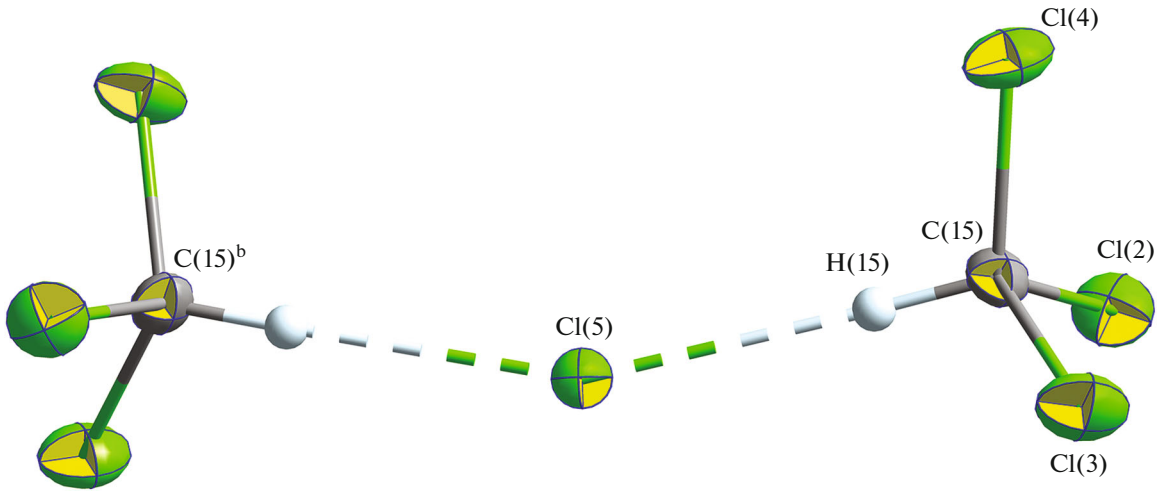

Fig. 4. Triad $[Cl_3C–H\cdots Cl\cdots H–CCl_3]^-$ formed by the outer-sphere Cl^- anion and solvate molecules $CHCl_3$. Ellipsoids of 50% probability. Symmetry transforms: [b] $1 - x, y, 1/2 - z$.

$C_1–X\cdots X$ and $C_2–X\cdots X$ angles ($\theta_1 \approx \theta_2$) in the structural $C_1–X\cdots X–C_2$ fragment, which can take both *cis* and *trans* configuration. For the second type, the angle is $\theta_1 \approx 180°$, while $\theta_2 \approx 90°$. In our case, the C(15)–Cl(4)···Cl(3)[a]–C(15)[a] structural fragment adopts the configuration close to the L-shaped one: the angles are $\theta_1 = 171.7°$ and $\theta_2 = 114.2°$, which is consistent with the second type of Cl···Cl interactions. The interhalogen interactions involving pairs of different halogen atoms (heterointeraction) should also be mentioned [34, 35].

The thermal behavior of complex **I** was studied by the STA method in an argon atmosphere with the simultaneous detection of the TG and DSC curves (Fig. 6). The compound is thermally stable up to ~89°C. The TG curve shows stepwise mass loss indicating that the thermal destruction process is multistage (Fig. 6*a*). The first step (~89–144°C) of a 15.45% mass loss corresponds to the complete desolvation of complex **I** (calcd. 15.46%). The inflection point at 118°C divides the discussed step into two unequal regions (slightly sloping and steeply descending), indicating a jump in an increase in the mass loss rate, which can be due to the melting of the sample. In the discussed temperature range, the DSC curve (Fig. 6*b*) includes two endoeffects with extremes at 109.2 and 129.7°C. The first extreme was attributed to sample melting (the extrapolated m.p. 98.0°C), and the second extreme is caused by the liberation of the solvate $CHCl_3$ molecules (extrapolated temperature of the process 122.3°C).

The region of the TG curve in a range of ~144–172°C is characterized by the stabilization of the sample weight followed by reaching the steeply descending thermolysis stage of the nonsolvated form of the complex (~172–311°C). The endoeffect at 194.2°C corresponds to the very beginning of the new step of mass loss on the DSC curve and was assigned to melting of the nonsolvated form of complex **I** (the extrapolated m.p. 190.0°C; for the independent determination in a capillary, melting was established in the range of 190.0–192.0°C). The total mass loss in the discussed region of the TG curve with an inflection point at 236.0°C is 42.86%, indicating a complicated character of thermolysis of the studied compound: simultaneously at the cationic and anionic moieties, which is accompanied by the reduction of gold to the elemental state and formation of AgCl (calcd. 47.45%). The corresponding fragment of the DSC curve exhibits two endoeffects at 216.5 and 263.1°C caused by the sequential thermal transformations of the substance (extrapolated temperatures of the processes are 207.8 and 261.8°C).

The final region of the TG curve (~311–1000°C) shows the smooth mass loss (9.31%) due to the desorption of volatile thermolysis products (7.01%) and reduction of elemental silver from AgCl (2.30%). At the end of thermolysis at 1100°C, the residual weight equal to 32.36% is well consistent with the calculated value for reduced gold and silver (32.50%). When the crucible was opened, fine light yellow balls representing a gold–silver alloy were observed on the bottom (Fig. 6*c*). The endoeffect with an extreme at 1043.9°C caused by the melting of the reduced metals (the extrapolated m.p. 1040.2°C) is detected in the high-temperature range of the DSC curve. The last value falls on the range between the melting points of gold and silver (1064.18 and 961.78°C, respectively [36]). An analysis of the state diagram of the Au–Ag binary metallic system [37] makes it possible to conclude more certainly that the above presented extrap-

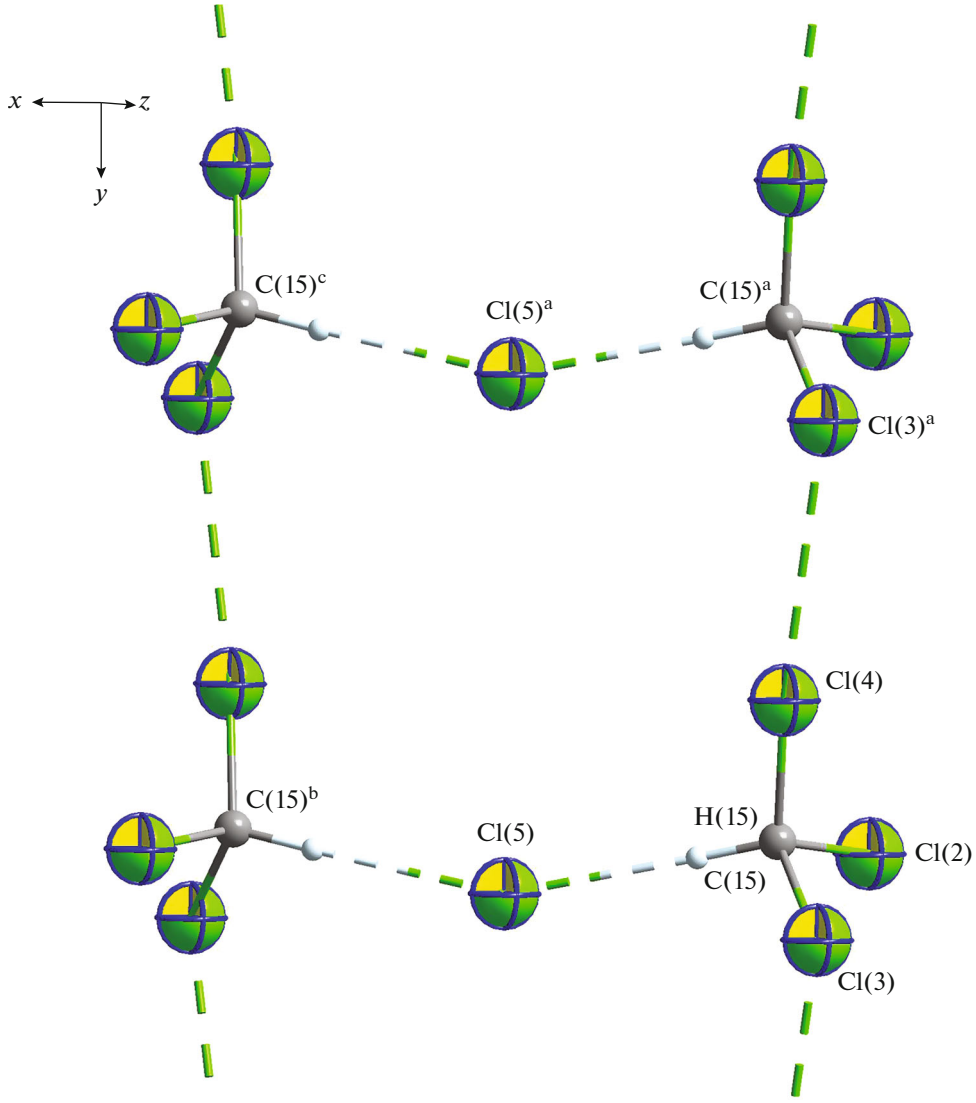

Fig. 5. Fragment of the anion-molecular pseudopolymeric ribbon $([Cl_3C{-}H{\cdots}Cl{\cdots}H{-}CCl_3]^-)_n$ formed by the solvated anion Cl^-; the Cl···Cl interaction and hydrogen bond between the $CHCl_3$ molecules and outer-sphere anion Cl^- are shown by dashed lines. Ellipsoids of 50% probability. Symmetry transforms: [a] $x, y-1, z$; [b] $1-x, y, 1/2-z$; [c] $1-x, y-1, 1/2-z$.

olated m.p. corresponds to an alloy with the atomic ratio of the components Au : Ag = 2 : 1.

Thus, the efficient capability of binding gold(III) to the solid phase from solutions with a high level of salinity (5.15 M solution of NaCl) was found for hexanuclear silver(I) *cyclo*-hexamethylenedithiocarbamate. The double Au(III)–Ag(I) solvated complex $[Au\{S_2CN(CH_2)_6\}_2]_2[AgCl_2]Cl{\cdot}2CHCl_3$ (**I**) was crystallized from an acetone–chloroform (1 : 1) solution of the heterogeneous reaction products as a form of binding $[AuCl_4]^-$. According to the XRD data, the synthesized compound is characterized by the complicated supramolecular structure containing two oppositely charged pseudo-polymeric subsystems $(\{[Au(HmDtc)_2]_2[AgCl_2]\}^+)_n$ and $([Cl_3C{-}H{\cdots}Cl{\cdots}H{-}CCl_3]^-)_n$. The secondary interactions (Ag···S, Au···Cl, and Cl···Cl) and hydrogen bonds C–H···Cl play the determining role in the formation of these subsystems. The study of the thermal behavior of complex **I** made it possible to establish the character of thermolysis and conditions for the quantitative regeneration of the metals.

ACKNOWLEDGMENTS

Elemental analysis was carried out on a Carlo Erba EA 1108 elemental analyzer at the Center for Collective Use "Physical Methods of Investigation" of Kurnakov Institute

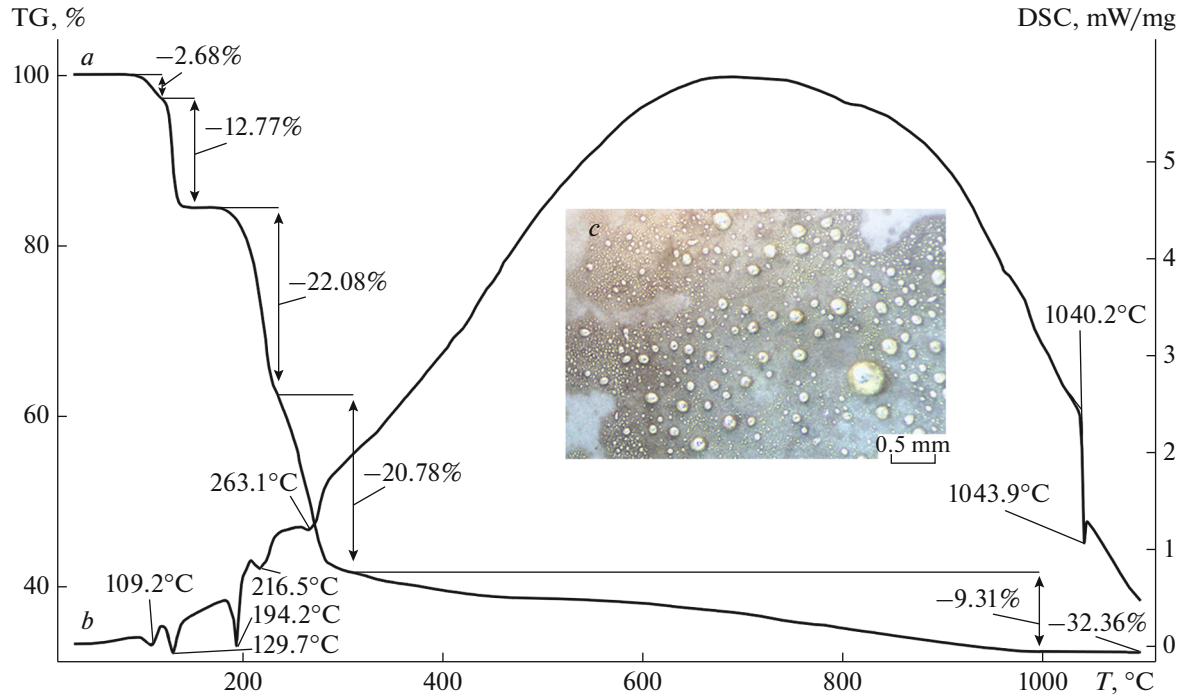

Fig. 6. (*a*) TG and (*b*) DSC curves for complex **I** and (*c*) the enlarged plan of the crucible bottom after the end of thermolysis.

of General and Inorganic Chemistry (Russian Academy of Sciences) supported by state assignment of Kurnakov Institute of General and Inorganic Chemistry (Russian Academy of Sciences) in the area of basic research.

CONFLICT OF INTEREST

The authors declare that they have no conflicts of interest.

OPEN ACCESS

REFERENCES

1. Hussain, S.T., Bakar, S.A., Saima, B.B., and Muhammad, B., *Appl. Surf. Sci.*, 2012, vol. 258, p. 9610.
2. Ehsan, M.A., Khaledi, H., Tahir, A.A., et al., *Thin Solid Films*, 2013, vol. 536, p. 124.
3. Mothes, R., Petzold, H., Jakob, A., et al., *Inorg. Chim. Acta*, 2015, vol. 429, p. 227.
4. Mothes, R., Jakob, A., Waechtler, T., et al., *Eur. J. Inorg. Chem.*, 2015, no. 10, p. 1726.
5. Jiang, F., Tian, Q., Tang, M., et al., *CrystEngComm*, 2011, vol. 13, no. 24, p. 7189.
6. Liu, W., Zhang, J., Peng, Z., et al., *Coll. Surf. A*, 2018, vol. 544, p. 111.
7. Li, C., Zhang, Y., Wang, M., et al., *Biomaterials*, 2014, vol. 35, no. 1, p. 393.
8. Zhang, Y., Hong, G., Zhang, Y., et al., *ACS Nano*, 2012, vol. 6, no. 5, p. 3695.
9. Zhao, G.J. and Stevens, S.E., *Biometals*, 1998, vol. 11, no. 1, p. 27.
10. Korneeva, E.V., Loseva, O.V., Smolentsev, A.I., and Ivanov, A.V., *Russ. J. Gen. Chem.*, 2018, vol. 88, no. 8, p. 1680. https://doi.org/10.1134/S1070363218080200
11. Korneeva, E.V., Smolentsev, A.I., Antzutkin, O.N., and Ivanov, A.V., *Russ. Chem. Bull. Int. Ed.*, 2019, vol. 68, no. 1, p. 40. https://doi.org/10.1007/s11172-019-2413-7
12. Teske, C.L., Hansen, A.-L., Weihrich, R., et al., *Chem. Eur. J.*, 2019, vol. 25, no. 27, p. 6763.
13. Berillo, D., *J. Clean. Prod.*, 2020, vol. 247, p. 119089.
14. Pohanka, M., *Mini-Rev. Med. Chem.*, 2021, vol. 21, no. 9, p. 1085.
15. Mäkelä M., Hatanpää T., Mizohata, K., et al., *Chem. Mater.*, 2017, vol. 29, no. 14, p. 6130.

16. Yang, J. and Ying, J.Y., *Chem. Commun.*, 2009, no. 22, p. 3187.

17. Korneeva, E.V., Ivanov, A.V., Gerasimenko, A.V., et al., *Russ. J. Gen. Chem.*, 2019, vol. 89, no. 8, p. 1642. https://doi.org/10.1134/S1070363219080152

18. Byr'ko, V.M., *Ditiokarbamaty* (Dithiocarbamates), Moscow: Nauka, 1984.

19. *APEX2 (Version 1.08), SAINT (Version 7.03), SADABS (Version 2.11)*, Madison: Bruker. AXS Inc., 2004.

20. Sheldrick, G.M., *Acta Crystallogr, Sect. C: Struct. Chem.*, 2015, vol. 71, no. 1, p. 3.

21. Loseva, O.V., Rodina, T.A., Ivanov, A.V., et al., *Russ. J. Coord. Chem.*, 2018, vol. 44, no. 10, p. 604. https://doi.org/10.1134/S107032841810007X

22. John Wiley & Sons, Inc. SpectraBase; SpectraBase Compound ID=5Zceg8XzL6u https://spectrabase.com/compound/5Zceg8XzL6u (request date: December 21, 2020).

23. John Wiley & Sons, Inc. SpectraBase; SpectraBase Compound ID=DiJQuAXLpJE https://spectrabase.com/compound/DiJQuAXLpJE (request date: December 21, 2020).

24. Tarasevich, B.N., *Osnovy IK spektroskopii s preobrazovaniem Fur'e. Podgotovka prob v IK spektroskopii* (Fundamentals of Fourier Transform IR Spectroscopy. Sample Preparation for IR Spectroscopy), Moscow: MGU, 2012.

25. Fabretti, A.C., Forghieri, F., Giusti, A., et al., *Spectrochim. Acta, Part A*, 1984, vol. 40, no. 4, p. 343.

26. Bocian, D.F., Pickett, H.M., Rounds, T.C., and Strauss, H.L., *J. Am. Chem. Soc.*, 1975, vol. 97, no. 4, p. 687.

27. Entrena, A., Campos, J., Gomez, J.A., et al., *Org. Chem.*, 1997, vol. 62, no. 2, p. 337.

28. Boessenkool, I.K. and Boeyens, J.C.A., *J. Cryst. Mol. Struct.*, 1980, vol. 10, nos. 1–2, p. 11.

29. Alcock, N.W., *Adv. Inorg. Chem. Radiochem.*, 1972, vol. 15, no. 1, p. 1.

30. Bondi, A., *J. Phys. Chem.*, 1964, vol. 68, no. 3, p. 441.

31. Reddy, C.M., Kirchner, M.T., Gundakaram, R.C., et al., *Chem. Eur. J.*, 2006, vol. 12, no. 8, p. 2222.

32. Awwadi, F.F., Willett, R.D., Peterson, K.A., and Twamley, B., *Chem. Eur. J.*, 2006, vol. 12, no. 35, p. 8952.

33. Hathwar, V.R., Roopan, S.M., Subashini, R., et al., *J. Chem. Sci.*, 2010, vol. 122, no. 5, p. 677.

34. Usoltsev, A.N., Korobeynikov, N.A., Novikov, A.S., et al., *Inorg. Chim. Acta*, 2020, vol. 513, p. 119932.

35. Podsiadło, M. and Katrusiak, A., *J. Phys. Chem. B*, 2008, vol. 112, no. 17, p. 5355.

36. Lidin, R.A., Andreeva, L.L., and Molochko, V.A., *Konstanty neorganicheskikh veshchestv: spravochnik* (Characteristics of Inorganic Substances), Moscow: Drofa, 2008.

37. *Diagrammy sostoyaniya dvoinykh metallicheskikh sistem: spravochnik* (Phase Diagrams of Binary Metallic Systems), Lyakishev, N.P., Ed., Moscow: Mashinostroenie, 1996.

Translated by E. Yablonskaya